

Robust Image Registration with Absent Correspondences in Pre-operative and Follow-up Brain MRI Scans of Diffuse Glioma Patients

Tony C. W. Mok and Albert C. S. Chung

The Hong Kong University of Science and Technology, Hong Kong, China
{cwmokab, achung}@cse.ust.hk

Abstract. Registration of pre-operative and follow-up brain MRI scans is challenging due to the large variation of tissue appearance and missing correspondences in tumour recurrence regions caused by tumour mass effect. Although recent deep learning-based deformable registration methods have achieved remarkable success in various medical applications, most of them are not capable of registering images with pathologies. In this paper, we propose a 3-step registration pipeline for pre-operative and follow-up brain MRI scans that consists of 1) a multi-level affine registration, 2) a conditional deep Laplacian pyramid image registration network (cLapIRN) with forward-backward consistency constraint, and 3) a non-linear instance optimization method. We apply the method to the Brain Tumor Sequence Registration (BraTS-Reg) Challenge. Our method achieves accurate and robust registration of brain MRI scans with pathologies, which achieves a median absolute error of 1.64 mm and 88% of successful registration rate in the validation set of BraTS-Reg challenge. Our method ranks 1st place in the 2022 MICCAI BraTS-Reg challenge.

Keywords: Absent correspondences · Patient-specific registration · Deformable registration

1 Introduction

Registration of pre-operative and follow-up images is crucial in evaluating the effectiveness of treatment for patients suffering from diffuse glioma. However, this registration problem is challenging due to the missing correspondences and mass effect caused by resected tissue. While many recent deep learning-based deformable registration algorithms [21,2,3,10,9,13,14,15] are available, only a few learning-based methods [5] address the missing correspondences problem. In this paper, we propose a 3-step registration pipeline for pre-operative and follow-up brain MRI scans that consists of 1) a multi-level affine pre-alignment, 2) a conditional deep Laplacian pyramid image registration network (cLapIRN) with forward-backward consistency constraint [17,16,18], and 3) a non-linear instance optimization with inverse consistency. We validate the method using the pre-operative and follow-up images brain MRI scans in the Brain Tumor Sequence Registration Challenge (BraTS-Reg) challenge [1].

2 Related Work

Accurate registration of pre-operative and post-recurrence brain MRI scans is crucial to the treatment plan and diagnosis of intracranial tumors, especially brain gliomas [7,20]. To better interpret the location and extent of the tumor and its biological activity after resection, the dense correspondences between pre-operative and follow-up structural brain MRI scans of the patient first need to be established. However, deformable registration between the pre-operative and follow-up scans, including post-resection and post-recurrence, is challenging due to possible large deformations and absent correspondences caused by tumor’s mass effects [4], resection cavities, tumor recurrence and tissue relaxation in the follow-up scans. While recent deep learning-based deformable registration (DLDR) methods [2,10,9,6,13] have achieved remarkable registration performance in many medical applications, these registration approaches often ignored the absent correspondence problem in the pre-operative and post-recurrence images. To address this issue, we extend our deep learning-based method described in [17] by introducing affine pre-alignment and non-linear instance optimization as post-processing to our method. DIRAC leverages conditional Laplacian Pyramid Image Registration Networks (cLapIRN) [16] as the backbone network, jointly estimates the bidirectional deformation fields and explicitly locates regions with absent correspondence. By excluding the regions with absent correspondence in the similarity measure during training, DIRAC improves the target registration error of landmarks in pre-operative and follow-up images, especially for those near the tumour regions.

3 Methods

We propose a 3-step registration pipeline for pre-operative and follow-up brain MRI scans which consists of 1) a gradient descent-based affine registration method, 2) a deformable image registration method with absent correspondence (DIRAC), and 3) a non-linear instance optimization method. Let B and F be the pre-operative (baseline) scan B and post-recurrence (follow-up) scan defined over a n -D mutual spatial domain $\Omega \subseteq \mathbb{R}^n$. Our goal is to establish a dense non-linear correspondence between the pre-operative scan and the post-recurrence scan of the same subject. In this paper, we focus on 3D registration, i.e., $n = 3$ and $\Omega \subseteq \mathbb{R}^3$.

3.1 Affine Registration

Although all MRI scans provided by the challenge are rigidly registered to the same anatomical template [1], we found that there are large linear misalignments between the pre-operative and follow-up images in cases suffering from serious tumor mass effect. To factor out the possible linear misalignment between MRI scans B and F , we register T1-weighted B and F scans using the iterative affine registration method.

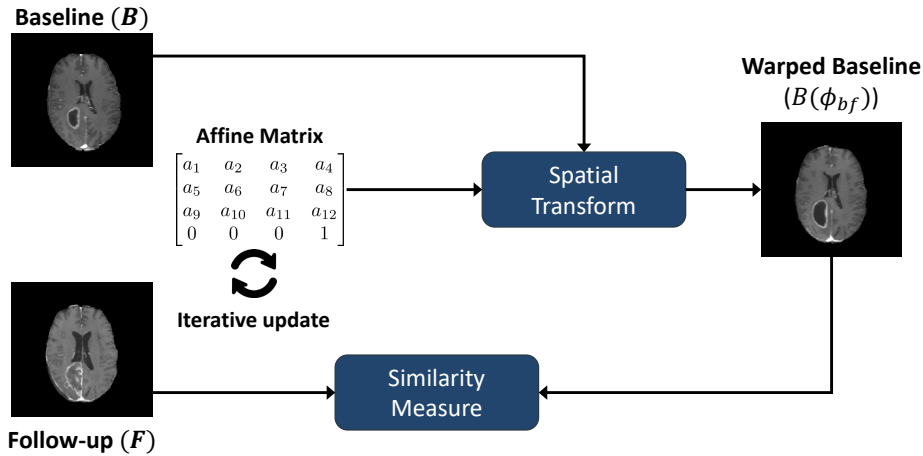


Fig. 1. Overview of the affine registration (Step 1). Our method optimizes the affine matrix using instance optimization. Only the baseline scan registered to the follow-up scan is shown for brevity.

Figure 1 depicts the overview of the affine registration. The affine registration method starts by initializing two identity matrices as initial affine transformation and creating image pyramids with N_{level} levels using trilinear interpolation for B and F . Then, we iteratively optimize the solutions by minimizing a suitable distance measure that quantifies alignment quality using the Adam optimizer [11] and a coarse-to-fine multi-resolution iteratively registration scheme. In this step, we use the Normalized Gradient Fields (NGF) distance measure [8]. Formally, the NGF is defined as:

$$\text{NGF}(B, F) = \int_{\Omega} 1 - \frac{\langle \nabla B, \nabla F \rangle^2}{\|\nabla B\|_{\epsilon}^2 \|\nabla F\|_{\epsilon}^2} \quad (1)$$

where $\langle x, y \rangle := x^{\top} y$, $\|x\|_{\epsilon} = \sqrt{x^{\top} x + \epsilon}$ and ϵ is an edge parameter controlling the level of influence of image gradients. The value of NGF is minimized when the gradients of B and F are aligned. The result with the minimal distance measure is selected as intermediate result.

3.2 Unsupervised Deformable Registration with Absent Correspondences Estimation

Assume that baseline scan B and follow-up scan F are affinely aligned in step 1 such that the main source of misalignment between B and F is non-linear, we then apply DIRAC [17] to further align B and F in an bidirectional manner. Since multi-parametric MRI sequences of each time-point, including T1 contrast-enhanced (T1ce), T2, T2 Fluid Attenuated (Flair) and T1-weighted (T1), are provided for each case in the BraTS-Reg challenge, we utilize all MRI modalities

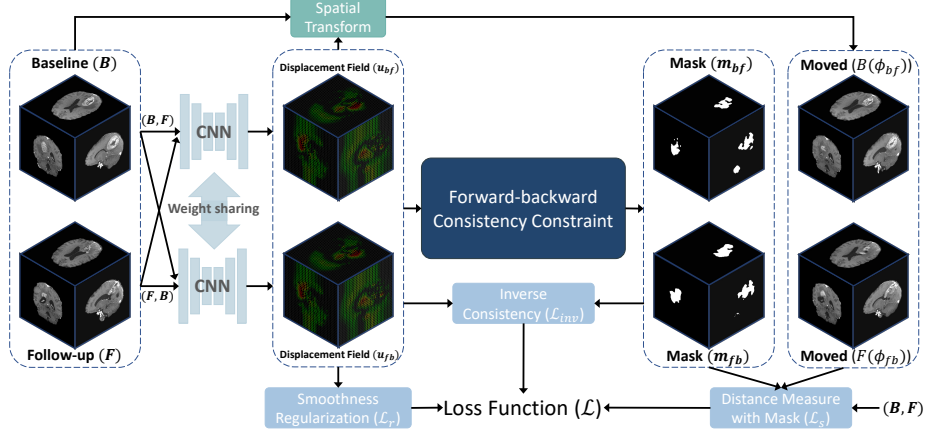


Fig. 2. Overview of the proposed deformable image registration method with absent correspondence. Our method jointly estimates the bidirectional deformation fields and locates regions with absent correspondence (denoted as mask). The regions with absent correspondence are excluded in the similarity measure during training. For brevity, the magnitude loss of the masks is omitted in the figure.

of the brain MRI scans in this step, i.e., B and F are 4-channel pre-operative and post-recurrence scans, respectively. Specifically, we parameterize the problem with a function $f_\theta(F, B) = (\mathbf{u}_{fb}, \mathbf{u}_{bf})$ cLapIRN [16], where θ is a set of learning parameters and \mathbf{u}_{bf} represents the displacement field that transform B to align with F , i.e., $B(x + \mathbf{u}_{bf}(x))$ and $F(x)$ define similar anatomical locations for each voxel $x \in \Omega$ (except voxels with absent correspondence). Figure 2 illustrates the overview of DIRAC. DIRAC leverages the bidirectional displacement fields and a forward-backward consistency locate regions with absent correspondence and excludes them in the similarity measure during training phase.

Forward-Backward Consistency Given the deformation fields $\phi_{bf} = Id + \mathbf{u}_{bf}$ and $\phi_{fb} = Id + \mathbf{u}_{fb}$, where Id is the identity transform and \mathbf{u} is the corresponding displacement vector field, we calculate the forward-backward error δ_{bf} for B to F as:

$$\delta_{bf}(x) = |\mathbf{u}_{bf}(x) + \mathbf{u}_{fb}(x + \mathbf{u}_{bf}(x))|_2. \quad (2)$$

Based on the observation that regions without true correspondences would have higher forward-backward error in solutions, we create a mask m_{bf} and mark $m_{bf}(x) = 1$ whenever the forward-backward error $\delta_{bf}(x)$ is larger than the pre-defined threshold $\tau_{bf}(x)$. The pre-defined threshold is defined as:

$$\tau_{bf} = \sum_{x \in \{x | F(x) > 0\}} \frac{1}{N_f} (|\mathbf{u}_{bf}(x) + \mathbf{u}_{fb}(x + \mathbf{u}_{bf}(x))|_2) + \alpha, \quad (3)$$

Table 1. Parameters used in the registration pipeline. NCC-SP: Negative Local Cross-correlation with Similarity Pyramid.

Parameters	Methods		
	Affine	DIRAC	Inst. Opt.
Input MRI sequences	T1ce	T1,T1ce,T2,Flair	T1ce,T2
Number of levels N_{level}	3	3	5
Max. image dimension N_{max}	(64, 64, 40)	(160, 160, 80)	(240, 240, 155)
Min. image dimension N_{min}	(16, 16, 16)	(40, 40, 20)	(80, 80, 80)
Learning rate per level	[1e-2, 5e-3, 2e-3]	[1e-4, 1e-4, 1e-4]	[1e-2, 5e-3, 5e-3, 3e-3, 3e-3]
Max. iteration per level N_{iter}	[90, 90, 90]	-	[150, 100, 100, 100, 50]
Distance measure	NGF($\epsilon = 0.01$)	NCC-SP($w = 7$)	NCC($w = 3$)
Max. number of grid points	-	$160 \times 160 \times 80$	$64 \times 64 \times 64$
Min. number of grid points	-	$40 \times 40 \times 20$	$32 \times 32 \times 32$
Weight of Inverse consistency λ_{inv}	-	[0.5, 0.5, 0.5]	[1.0, 2.0, 4.0, 8.0, 10.0]

where α is set to 0.015. Then, we create a binary mask \mathbf{m}_{bf} to mark voxels with absent correspondence as follows:

$$\mathbf{m}_{bf}(x) = \begin{cases} 1, & \text{if } (\mathbf{A} \star \delta_{bf})(x) \geq \tau_{bf} \\ 0, & \text{otherwise} \end{cases} \quad (4)$$

where \mathbf{A} denotes an averaging filter of size $(2p+1)^3$ and \star denotes a convolution operator with zero-padding p .

Objective Function The objective function \mathcal{L} of DIRAC is defined as follows:

$$\mathcal{L} = (1 - \lambda_{reg})\mathcal{L}_s + \lambda_{reg}\mathcal{L}_r + \lambda_{inv}\mathcal{L}_{inv} + \lambda_m(|m_{bf}| + |m_{fb}|) \quad (5)$$

where the masked dissimilarity measure \mathcal{L}_s and the masked inverse consistency loss \mathcal{L}_{inv} are defined as:

$$\mathcal{L}_s = \mathcal{L}_{\text{sim}}(B, F(\phi_{fb}), (1 - m_{fb})) + \mathcal{L}_{\text{sim}}(F, B(\phi_{bf}), (1 - m_{bf})) \quad (6)$$

and

$$\mathcal{L}_{inv} = \sum_{x \in \Omega} (\delta_{bf}(x)(1 - m_{bf}(x)) + \delta_{fb}(x)(1 - m_{fb}(x))). \quad (7)$$

In this step, we use masked negative local cross-correlation (NCC) with similarity pyramid [18] as the dissimilarity function. To encourage smooth solutions and penalize implausible solutions, we adopt a diffusion regularizer $\mathcal{L}_r = \|\nabla \mathbf{u}_{bf}\|_2^2 + \|\nabla \mathbf{u}_{fb}\|_2^2$ during training. We set λ_{reg} and λ_m to 0.4 and 0.01, respectively. For more details, we recommend interested reader also refer to [17].

3.3 Non-rigid Instance Optimization

Due to insufficient amount of training data and discrepancy in distributions between training and test set, the learning-based method in step 2 may produce

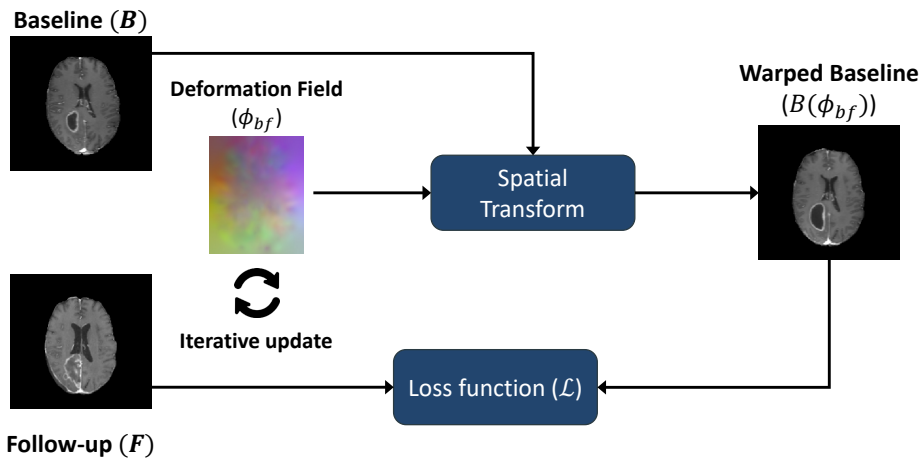


Fig. 3. Overview of the non-rigid instance optimization (Step 3). Initially, the deformation field is initialized with the solution estimated from Step 2. The bidirectional deformation fields are jointly updated using Adam optimizer. For brevity, only baseline scan register to the follow-up scan is shown in the figure.

Table 2. Results on the training set in the BraTS-Reg challenge. MAE_{median} and MAE_{mean} denote the average of median absolute error and mean absolute error of the transformed coordinates and the manually defined coordinates (in millimetre), respectively. Initial: Results before registration.

Methods	MAE_{median}	MAE_{mean}	Robustness
Initial	8.20 ± 7.62	8.65 ± 7.31	-
Ours	2.98 ± 6.25	4.64 ± 11.06	0.78 ± 0.23

biased solutions, especially in cases with small initial misalignment. As such, we introduce a non-rigid instance optimization step to further improve the robustness and registration accuracy of solutions from the previous step. Figure 3 shows the overview of the non-rigid instance optimization. In the final step, the non-parametric deformation is controlled by the same objective function in 5, except we use NCC as the distance measure. The smoothness regularization coefficients λ_{reg} for each level are set to $[0.25, 0.3, 0.3, 0.35, 0.35]$, respectively. The displacement fields are discretized with trilinear interpolation defined on a uniform control point grid with a fixed number of points. We use an Adam optimizer together with multi-level continuation to avoid local minima.

3.4 Hyperparameters

The hyperparameters of our 3-step approach are summarized in Table 1.

Table 3. Results on the validation set in the BraTS-Reg challenge. MAE and Robustness denote the average of median absolute error and mean absolute error of the transformed coordinates and the manually defined coordinates (in millimetre), respectively. Robustness measures the successful-rate of the registered landmarks. Affine, A-DIRAC and A-DIRAC-IO denote affine registration, DIRAC with affine pre-alignment and our proposed 3-step method, respectively. Initial: Results before registration.

Case	Initial	Affine		A-DIRAC		A-DIRAC-IO	
	MAE	MAE	Robustness	MAE	Robustness	MAE	Robustness
Case 141	13.50	4.26	1.00	1.94	1.00	1.62	1.00
Case 142	14.00	6.12	0.88	3.07	1.00	1.88	1.00
Case 143	16.00	8.98	1.00	2.63	1.00	1.14	1.00
Case 144	15.00	9.52	0.88	3.10	1.00	2.56	1.00
Case 145	17.00	5.14	1.00	2.09	1.00	1.13	1.00
Case 146	17.00	5.74	1.00	1.84	1.00	1.94	1.00
Case 147	1.50	2.03	0.45	2.17	0.60	1.64	0.55
Case 148	3.50	2.90	0.75	1.71	0.90	1.43	0.90
Case 149	9.00	2.22	1.00	1.94	1.00	1.56	1.00
Case 150	4.00	3.65	0.53	2.87	0.63	1.27	0.74
Case 151	3.00	2.13	0.5	1.39	0.75	1.18	0.85
Case 152	5.00	2.11	0.95	1.45	0.84	1.42	0.95
Case 153	2.00	2.04	0.33	1.44	0.67	1.80	0.67
Case 154	2.00	2.61	0.25	2.02	0.4	1.98	0.55
Case 155	2.00	3.09	0.21	2.43	0.37	1.70	0.53
Case 156	7.00	2.84	1.00	2.29	1.00	1.45	1.00
Case 157	10.00	4.90	0.90	2.67	1.00	1.66	1.00
Case 158	4.50	3.48	0.40	1.39	0.80	1.13	1.00
Case 159	6.00	7.28	0.36	2.25	1.00	2.28	1.00
Case 160	4.00	2.55	0.7	2.29	0.80	1.94	0.90
Mean	7.80	4.18	0.70	2.15	0.84	1.64	0.88
Std	5.62	2.30	0.29	0.54	0.21	0.39	0.17
Median	5.50	3.28	0.81	2.13	0.95	1.63	1.00

4 Experiments

Implementation Our proposed method is implemented with PyTorch 1.8 [19] and trained with an Nvidia Titan RTX GPU and an Intel Core (i7-4790) CPU. We build DIRAC on top of the official implementation of cLapIRN available in [12]. We adopt Adam optimizer [11] with a fixed learning rate $1e-4$ and train it from scratch with the training data from the BraTS-Reg challenge.

Measurements We quantitatively evaluate our method based on the average of the median absolute error (MAE) and robustness of anatomical landmarks. Specifically, the MAE is defined as:

$$\text{MAE} = \text{Median}_{l \in L}(|x_l^B - \hat{x}_l^B|), \quad (8)$$

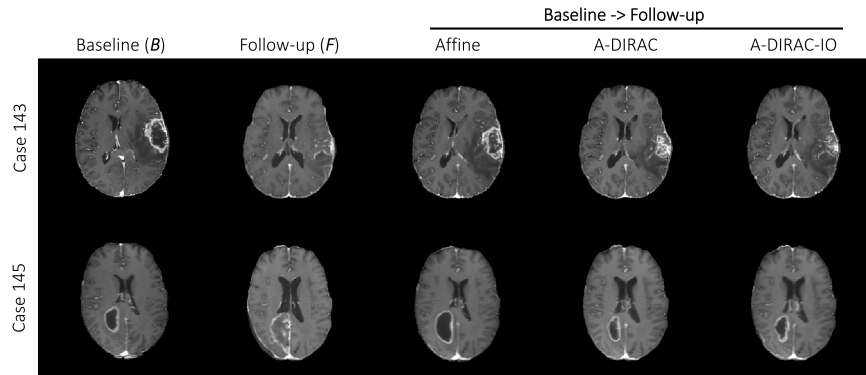


Fig. 4. Example axial T1ce MR slices of resulting warped images (B to F) from affine, A-DIRAC and A-DIRAC-IO registration methods.

where x_l^B is the l -th estimated anatomical landmark in the baseline scan and \hat{x}_l^B is the l -th groundtruth landmark in the baseline scan. The robustness is defined as the ratio of landmarks with improved MAE after registration to all landmarks, following the definition in [1].

Results For each case in the training and validation set of the BraTS-Reg challenge, we register the pre-operative image scan to the follow-up image scan and use the resulting deformation field to transform the manually defined landmarks in the follow-up scan. In total, there are 140 and 20 pairs of pre-operative and follow-up image scans in the training and validation set, respectively. We follow the evaluation pipeline of the BraTS-Reg challenge and report the average median absolute error MAE and robustness of the training and validation set in Tables 2 and 3.

An example qualitative result is shown in Figure 4. The reduction of the registration error in the validation set in the pipeline is shown in Table 3. While the MRI scans are pre-registered to a common template, the average median error is reduced from 7.8 mm to 4.18 mm, indicating there exists a large linear misalignment between each case. Furthermore, the median error and robustness are consistently improved after each step, reaching to 1.64 mm average median error. Notably, our MAE is the lowest on the challenge’s validation leaderboard.

5 Conclusion

We proposed a 3-step registration method for pre-operative and follow-up brain tumor registration. The method was evaluated with the dataset provided by the BraTS-Reg challenge and ranked 1st place in the 2022 MICCAI BraTS-Reg challenge. By combining the pathological-aware deep learning-based method

and instance optimization, we demonstrated the follow-up scan could be accurately registered to the pre-operative scan with an average median absolute error of 1.64mm. Compared to conventional methods, our method inherits the runtime advantage from deep learning-based approaches and does not require any manual interaction or supervision, demonstrating immense potential in the fully-automated patient-specific registration. We left the further analysis of our method and the comparison to existing methods for future work.

References

1. Baheti, B., Waldmannstetter, D., Chakrabarty, S., Akbari, H., Bilello, M., Wiestler, B., Schwarting, J., Calabrese, E., Rudie, J., Abidi, S., et al.: The brain tumor sequence registration challenge: Establishing correspondence between pre-operative and follow-up mri scans of diffuse glioma patients. arXiv preprint arXiv:2112.06979 (2021)
2. Balakrishnan, G., Zhao, A., Sabuncu, M.R., Guttag, J., Dalca, A.V.: An unsupervised learning model for deformable medical image registration. In: Proceedings of the IEEE conference on computer vision and pattern recognition. pp. 9252–9260 (2018)
3. Dalca, A.V., Balakrishnan, G., Guttag, J., Sabuncu, M.R.: Unsupervised learning for fast probabilistic diffeomorphic registration. In: International Conference on Medical Image Computing and Computer-Assisted Intervention. pp. 729–738. Springer (2018)
4. Dean, B.L., Drayer, B.P., Bird, C.R., Flom, R.A., Hodak, J.A., Coons, S.W., Carey, R.G.: Gliomas: classification with mr imaging. *Radiology* **174**(2), 411–415 (1990)
5. Han, X., Shen, Z., Xu, Z., Bakas, S., Akbari, H., Bilello, M., Davatzikos, C., Niethammer, M.: A deep network for joint registration and reconstruction of images with pathologies. In: International Workshop on Machine Learning in Medical Imaging. pp. 342–352. Springer (2020)
6. Heinrich, M.P.: Closing the gap between deep and conventional image registration using probabilistic dense displacement networks. In: International Conference on Medical Image Computing and Computer-Assisted Intervention. pp. 50–58. Springer (2019)
7. Heiss, W.D., Raab, P., Lanfermann, H.: Multimodality assessment of brain tumors and tumor recurrence. *Journal of Nuclear Medicine* **52**(10), 1585–1600 (2011)
8. Hodneland, E., Lundervold, A., Rørvik, J., Munthe-Kaas, A.Z.: Normalized gradient fields and mutual information for motion correction of dce-mri images. In: 2013 8th International Symposium on Image and Signal Processing and Analysis (ISPA). pp. 516–521. IEEE (2013)
9. Hu, X., Kang, M., Huang, W., Scott, M.R., Wiest, R., Reyes, M.: Dual-stream pyramid registration network. In: International Conference on Medical Image Computing and Computer-Assisted Intervention. pp. 382–390. Springer (2019)
10. Kim, B., Kim, J., Lee, J.G., Kim, D.H., Park, S.H., Ye, J.C.: Unsupervised deformable image registration using cycle-consistent cnn. In: International Conference on Medical Image Computing and Computer-Assisted Intervention. pp. 166–174. Springer (2019)
11. Kingma, D.P., Ba, J.: Adam: A method for stochastic optimization. arXiv preprint arXiv:1412.6980 (2014)

12. Mok, T.C., Chung, A.: Official implementation of conditional deep laplacian pyramid image registration network. https://github.com/cwmok/Conditional_LapIRN, accessed: 01.03.2021
13. Mok, T.C., Chung, A.: Fast symmetric diffeomorphic image registration with convolutional neural networks. In: Proceedings of the IEEE/CVF conference on computer vision and pattern recognition. pp. 4644–4653 (2020)
14. Mok, T.C., Chung, A.: Large deformation image registration with anatomy-aware laplacian pyramid networks. In: International Conference on Medical Image Computing and Computer-Assisted Intervention. pp. 61–67. Springer (2020)
15. Mok, T.C., Chung, A.: Conditional deep laplacian pyramid image registration network in learn2reg challenge. In: International Conference on Medical Image Computing and Computer-Assisted Intervention. pp. 161–167. Springer (2021)
16. Mok, T.C., Chung, A.: Conditional deformable image registration with convolutional neural network. In: International Conference on Medical Image Computing and Computer-Assisted Intervention. pp. 35–45. Springer (2021)
17. Mok, T.C., Chung, A.: Unsupervised deformable image registration with absent correspondences in pre-operative and post-recurrence brain tumor mri scans. In: International Conference on Medical Image Computing and Computer-Assisted Intervention. pp. 25–35. Springer (2022)
18. Mok, T.C., Chung, A.C.: Large deformation diffeomorphic image registration with laplacian pyramid networks. In: International Conference on Medical Image Computing and Computer-Assisted Intervention. pp. 211–221. Springer (2020)
19. Paszke, A., Gross, S., Chintala, S., et al.: Automatic differentiation in pytorch. In: NIPS-W (2017)
20. Price, S.J., Jena, R., Burnet, N.G., Carpenter, T.A., Pickard, J.D., Gillard, J.H.: Predicting patterns of glioma recurrence using diffusion tensor imaging. *European radiology* **17**(7), 1675–1684 (2007)
21. de Vos, B.D., Berendsen, F.F., Viergever, M.A., Staring, M., Išgum, I.: End-to-end unsupervised deformable image registration with a convolutional neural network. In: Deep Learning in Medical Image Analysis and Multimodal Learning for Clinical Decision Support, pp. 204–212. Springer (2017)